A Study on Sulfide Stress Cracking Susceptibility of GMA Girth Welds in X80 Grade Pipes

YUJI KISAKA, NICK SENIOR, and ADRIAN P. GERLICH

The present work evaluates the SSC susceptibility of linepipe steel weld metals produced with various microstructures consisting of different ratios of intragranular (acicular) ferrite and grain boundary ferrite. It is shown that weld metal with high fractions of intragranular ferrite and low grain boundary ferrite passed SSC tests even though their hardness exceeded 250 HV, the widely accepted guideline to prevent SSC fracture initiation. Using a novel combination of hydrogen microprinting combined with SEM and TEM electron microscopy analysis techniques, the intragranular ferrite grain boundaries are shown to provide key hydrogen trapping sites which consist of fine grains and finely dispersed nano-scale carbide precipitates. The presence of a high fraction of trapping sites is suggested to account for the good SSC resistance coupled with high hardness, while increased grain boundary ferrite led to rejection during SSC testing due to inferior fracture toughness associated with coarser grains.

I. INTRODUCTION

THE use of high strength linepipes is motivated by various benefits including reduced construction costs (derived from transportation and welding) associated with reduced wall thickness, and operational costs permitted through increased gas pressure during normal operation. The girth welds for such pipelines simultaneously require strength overmatching, high fracture toughness, and low hardness, although these mechanical properties are potentially at odds with each other and may be difficult to achieve during construction. Furthermore, when new natural gas pipelines are constructed for severe sour service applications (containing highly pressured hydrogen sulfide gas), satisfying all performance requirements simultaneously is more difficult since lower hardness limits are imposed to avoid Sulfide Stress Cracking (SSC). National Association of Corrosion Engineers (NACE) standard MR0175/ISO 15156 and European Federation of Corrosion publication number 16 (EFC No.16), which have been applied as a common hardness guideline, require the maximum hardness of the materials to be below 250 HV regardless of pipe grade, based on experience and testing conducted more than 40 years ago.[1,2] This hardness limitation has been widely applied to not only base metals but also weld metals even though their chemical composition, microstructure, and mechanical properties may be different. The SSC susceptibility of base materials and weld metals has been investigated for a long time by many researchers.[3–12]

Some papers discussing SSC susceptibility for weld metals indicate that despite the requirements of standards, findings have suggested that SSC does not necessarily initiate even if the maximum hardness in weld metals exceeds 250 HV. For example, the SSC susceptibility of submerged arc weld (SAW) metals in API 5L X70 pipes was investigated by Beidokhti et al.,[13] who considered ten different weld metals with various manganese contents and acicular ferrite volume fractions. One of the results indicated that a sample characterized by low manganese and high acicular ferrite fraction content was able to pass the SSC test even though the maximum hardness value was approximately 260 HV. Also, the SSC susceptibility of reheated SAW metals, produced by performing gas metal arc (GMA) welding on SAW metals and involving a microstructure dominated by acicular ferrite, has been investigated by Kasuya et al.[14] This work evaluated the relationship between carbon equivalent (CE) for weld metals with varying chemical compositions and the critical hardness value for SSC initiation. The results indicate that although the hardness criterion based on a critical value of 250 HV follows NACE standard MR0175/ISO 15156 and EFC publication No.16 when CE is more than 0.32 pct, SSC does not initiate when the CE is less than 0.32 pct. Moreover, the hydrogen trapping mechanism in a SAW weld metal dominated by acicular ferrite was investigated using the hydrogen

YUJI KISAKA is with the University of Waterloo, Waterloo, Canada. NICK SENIOR is with the CanmetMATERIALS, Hamilton, Canada. ADRIAN P. GERLICH is with the University of Waterloo. Contact e-mail: ykisaka@uwaterloo.ca

microprint technique by Wang *et al.*[15] This technique reveals the hydrogen trap site distribution near the surface of test coupons by utilizing a reaction between silver bromide painted on a test sample and diffusible hydrogen present in the material. Their results show that hydrogen has a preferential distribution corresponding to the grain boundaries of acicular ferrite. This indicates that acicular ferrite can trap diffusible hydrogen through a fine grain structure, hence reducing SSC susceptibility. On the other hand, those prior studies had focused on SAW weld metals which depend highly on a slag system for controlling impurities and inclusions involved in hydrogen trapping. There are few reports for GMA welds which are widely used for girth welds in pipelines, where heat input is much lower compared to SAW.

Based on the past work, the critical hardness value to evaluate SSC susceptibility, especially in GMA welds, requires more detailed consideration. Furthermore, the roles of acicular ferrite in GMA weld metals should be investigated since the grain size may be quite different compared with SAW weld metals. Thus, the aims of this paper are to evaluate SSC susceptibility for GMA weld metals, which have various intragranular ferrite (IGF) volume fractions, and investigate the correlation between microstructure, hardness, and SSC resistance in GMA welds.

II. EXPERIMENT

The specimen list is shown in Table I and the fixtures and set up used during welding is illustrated in Figure 1. All specimens were produced by robotic GMA welding a U-shaped groove in butt joint configuration, in the flat position. Pipe segments from 1/8 circumferential sections of API 5L X80 grade pipe of 610 mm (24″) diameter and a 15.1 mm thickness was used as the base material, with sample lengths of approximately 230 mm. Since it is well known that titanium oxides act as nucleation sites for acicular ferrite in weld metals, the titanium content was varied in the weld metal using two kinds of welding consumables; wire "A" which did not include titanium, and wire "B" containing 0.06 wt pct. A third variant, designated "AA" was produced through *in-situ* alloying by adding a 0.2-mm-diameter titanium wire to the filler passes, where the wire was fixed by resistance spot welding every few centimeters in order to avoid being blown away by shielding gas and arc plasma. The oxygen content in the AA weld was also varied by utilizing two shielding gases; $Ar + 30$ pct CO_2 and $Ar + 50$ pct CO_2 (described as AA-30 and AA-50

respectively). The chemical compositions of the weld metals are also shown in Table I, and measured in accordance to ASTM E1019-11, E2097-12(modified), and E1479-99(2011). Multi-pass welding utilizing six passes was conducted by applying the following welding conditions for the wire current, voltage and feed speed; 290–320 A, 24.5–28.0 V, and 120 cm/min for the root pass, 280–310A, 24.5–28.0 V, and 70 cm/min for hot and filler pass, and 210–230 A, 21.5–25.0 V, and 30 cm/min for cap pass. Preheat and interpass temperatures were controlled by limiting them to 150 °C.

After welding, hardness testing and metallography were conducted in order to evaluate properties for all weld metals; samples were extracted from 40 mm away from the crater location at the end of welding bead for each specimen, respectively. The Vickers hardness of the weld metals were determined at 9.8 N load and 0.5 mm pitch, in which the sampling position was a line 2 mm from the bottom edge (inner diameter) of the pipe. After hardness testing, specimens were re-polished and etched with 5 pct Nital solution to observe the microstructure.

The volume fraction of IGF was quantified by point counting method, where a grid was drawn at a 10 μm pitch on micrographs taken at ×200 magnification (for a total of 896 cross points for each picture), and the number of intersections for each microstructure was counted with the average and standard deviation reported across five pictures for each specimen. In this paper, microstructures were distinguished as grain boundary ferrite (GBF), IGF (which was predominantly acicular ferrite, but could also include Widmanstätten ferrite + polygonal ferrite + bainitic ferrite), and bainite (B, upper and lower bainite).

SSC tests were conducted according to NACE standard MR0175/ISO 15156 and EFC No.16. Three specimens, measuring 15 mm in width, 115 mm long, and 5 mm thick, were extracted from each welded joint. These SSC specimens were cut from a position 2 mm from the inside surface of the base metals. The samples were then loaded in bending fixtures so that the weld metal on the inner side of the pipe wall was under tensile stress during SSC tests. The tests utilized NACE A solution (5.0 wt pct sodium chloride and 0.5 wt pct glacial acetic acid in distilled water) for SSC evaluation.[1] Three levels of applied stress were targeted (nominally 452, 480, and 509 MPa), which corresponded to 80, 85, and 90 pct of the actual yield stress for the base materials, while the joint A-30 was only tested at 480 MPa. 4-point and 3-point bending methods were employed to load the required stress. Initially, the AA-30 series was tested with a 4-point bending

Table I. Specimen List

| Specimen ID | Welding Wire | Shielding Gas | Chemical Composition in Weld Metals (Wt Pct) | | | | | | | | |
			C	Si	Mn	P	S	Al	Ti	O	N
A-30	Wire A	70 pct Ar-30 pct CO_2	0.082	0.48	1.69	< 0.010	< 0.005	< 0.01	0.01	0.029	0.0032
AA-30	Wire A + Ti wire	70 pct Ar-30 pct CO_2	0.082	0.53	1.72	< 0.010	< 0.005	< 0.01	0.04	0.026	0.0036
AA-50	Wire A + Ti wire	50 pct Ar-50 pct CO_2	0.079	0.47	1.63	< 0.010	< 0.005	< 0.01	0.03	0.027	0.0036
B-30	Wire B	70 pct Ar-30 pct CO_2	0.055	0.50	1.66	< 0.010	< 0.005	< 0.01	0.03	0.031	0.0039

method; however, one specimen failed by crack initiation from the fusion line, rather than the weld metal. Since the purpose of this paper is to investigate SSC susceptibility for weld metals, the method of load application was revised to the 3-point bending method for remaining specimens in order to ensure the highest stress concentration at the weld metal. Target deflections were calculated according to ASTM G39[16] and three specimens, loaded at the three levels of applied stress, were tested in a chamber simultaneously. The pH of the solution was monitored during the SSC test throughout the time of 720 hours.

It is known that the hydrogen microprint technique is one of the methods which can reveal hydrogen trapping sites in the microstructure by utilizing a reaction with silver bromide and hydrogen.[17–20] A specimen of 2 mm thickness was extracted from the AA-50 weld metal and was found to contain a marginally higher IGF volume fraction than the other welds (refer to Figure 2). The specimen was mounted with conductive resin and polished with # 600 grit paper. Then the specimen was connected to the cathode side of a galvanostat and immersed in 0.1 M NaOH at room temperature, where a Pt plate was used as counter electrode. The electrical charging was applied at a current density of 27 mA/cm^2 for approximately 110 hours to promote saturation at the surface. After charging, the specimen was re-polished quickly with 1 micron alumina paste then 1 μm diamond paste. The specimen was then covered by with liquid nuclear emulsion (Ilford L4 which contains AgBr of 0.11 μm, diluted with 1.4 mol/L NaNO$_2$ solution) with a wire loop method.[17–20] After drying for approximately 10 minutes, the specimen was heated up to 150 °C for 3 hours in order to promote a reaction between silver bromide and hydrogen. It was subsequently dipped into formalin (37 mass pct HCHO water solution) for 3 seconds for hardening, and immersed in a fixing solution (15 mass pct Na$_2$S$_2$O$_3$ with 1.4 mol/L NaNO$_2$ solution) for 5 minutes.
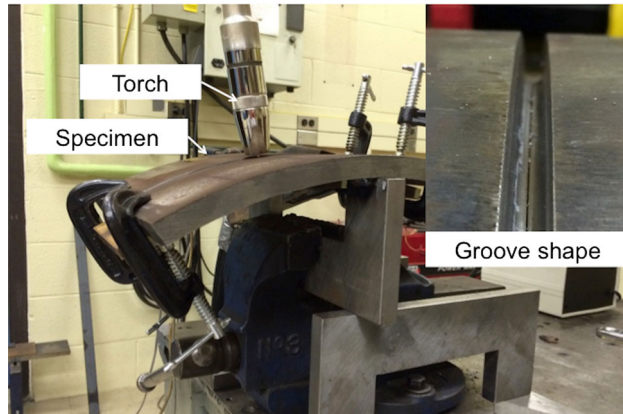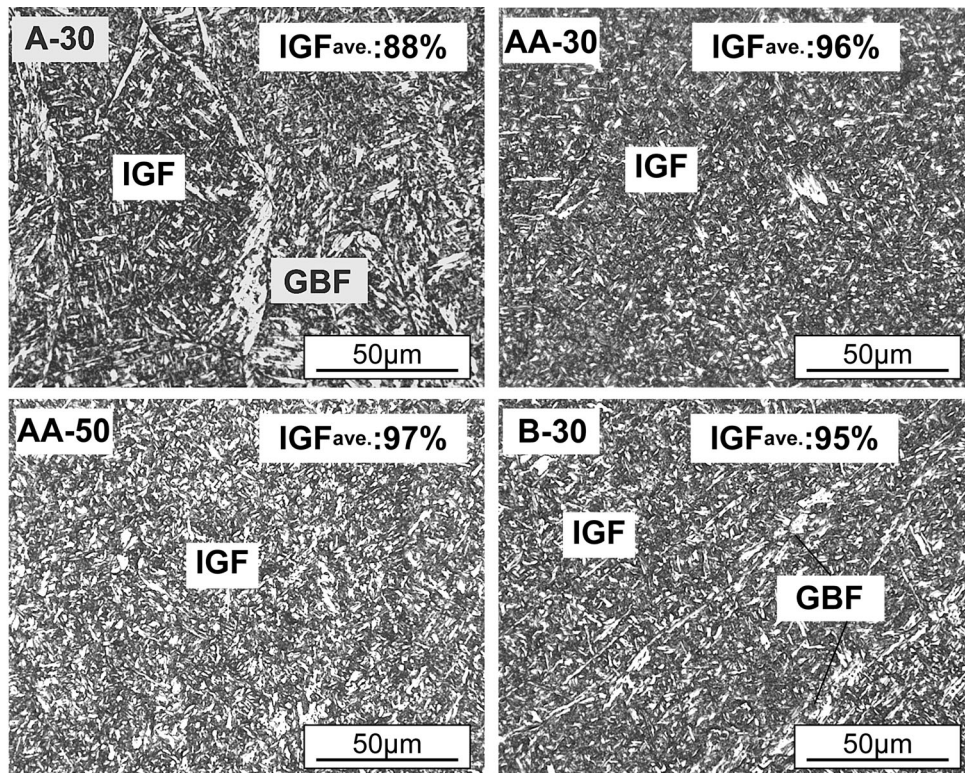

Fig. 1—Layout of pipe segment with backing fixture during welding.

IGF: Intragranular ferrite, GBF Grain boundary ferrite, IGFave: IGF volume fraction averaged by five pictures

Fig. 2—Optical micrographs of weld metal samples A-30, AA-30, AA-50, and B-30.

Through this process, silver particles precipitated on the surface, indicating the locations of hydrogen trapping sites. These were observed by scanning electron microscope (SEM) and energy dispersive X-ray spectrometry (EDS). Finally, the specimen surface was milled approximately 0.1 to 0.2 μm to remove the silver particles and surface deformation using a tilted ion beam, where an Ar ion beam was used for the milling for 60 seconds. Electron Back-Scattered Diffraction (EBSD) was performed on the same surface in order to reveal more detail regarding the locations of silver particles, in terms of grain boundary characteristics, using a step size of 0.6 μm, with an accelerating voltage of 20 kV. Data collection during EBSD involved fitting to within a mean angular deviation (MAD) factor of less than 0.6, and no further filtering was used to interpolate non-indexed points. Transmission electron microscopy (TEM) of the specimens was also performed an FEI Titan 80-300 LB, operated at 300 kV. Specimens for TEM were extracted using focused ion beam (FIB) milling, performed using a Zeiss NVision 40. This involved initially depositing a layer of tungsten to prevent excavating the material on the plane of the specimen. Further low energy milling was performed in steps at 10 and 5 kV to remove amorphous material from the surfaces. These specimens were used to observe nano-scale inclusions and dislocation structures in the weld metals.

III. RESULTS

Optical microphotographs for the weld metals studied are illustrated in Figure 2. It can be seen that intragranular ferrite (IGF), which here includes acicular ferrite or other microconstituents nucleated within the interior of prior austenite grains, is the most dominant structure for all welds. The volume fraction of IGF was quantified, by point counting, as 88 pct or more in each weld; the average and calculated standard deviation across five pictures for each specimen is also shown as IGFave and σ in Figure 2. The balance of the microconstituents aside from IGF was composed of GBF. It is worth noting is that Sample A-30 included a significantly lower IGF volume fraction (88 pct) than the other weld metals which ranged from 95 to 97 pct. This indicates that the fraction of GBF fraction in A-30 was significantly higher than the other specimens (12 pct, *vs* 3 to 5 pct).

The averaged specimen hardness results, before the SSC testing, always exceeded the 250 HV criterion limit of typical materials standards (Table II). SSC test results are summarized in the same table. The joints comprising weld metals A-30 and AA-30 series failed; however, all specimens for AA-50 series and B-30 series survived despite high hardness values exceeding 250 HV. It is noted that from these results, the influence of applied stress may not be directly correlated to crack susceptibility, although SSC initiation should be affected by applied stress level. The macrograph of the A-30 specimen after the SSC test is presented in Figure 3 as an example. The crack initiated at the weld metal and propagated through the bead center along the grain boundaries. Comparison of hardness values before and after SSC testing are also shown in Table III. For all specimens, hardness values after the SSC test are higher; in particular A-30 exhibited the most significant increase. Additionally, it can be noted that the hardness of specimens using welding consumable A exceeded that of welding consumable B.

The distribution of hydrogen trapping sites revealed by hydrogen microprint technique is illustrated in Figure 4. In this method, the locations of the silver particles are first revealed by EDS mapping; then the surface is cleaned by ion milling before EBSD mapping in order to remove surface layers strained by mechanical polishing. Milling also removes most of silver particles. After ion milling, the location mapped by EDS was also analyzed by EBSD; however, some locations where many silver particles were present had low indexing rates due to reduced ion milling rates. Figure 4(a) shows the SEM micrograph, while Figure 4(b) indicates the distribution of silver particles, which was obtained based on EDS mapping. Based on this result, it is clear that the particles distributed on the surface in Figure 4(a) are composed of silver. Figure 4(c) illustrates a result of EBSD analysis, where the color indicates phase

Table II. Results of Hardness Test for Weld Metals Before SSC Test and SSC Test Results

			Hardness, 2 mm from Pipe Bottom Surface, HV1		Results of SSC Tests	
Specimen ID	Welding Wire	Shielding gas	Maximum	Mean, $\pm \sigma$	Applied Stress (MPa)	Acceptability
A-30	Wire A	70 pct Ar-30 pct CO_2	258	251 ± 11.7	480	rejected
AA-30-1	Wire A + Ti wire	70 pct Ar-30 pct CO_2	295	273 ± 11.7	452	rejected
AA-30-2	Wire A + Ti wire	70 pct Ar-30 pct CO_2	295	273 ± 11.7	480	rejected
AA-30-3	Wire A + Ti wire	70 pct Ar-30 pct CO_2	295	273 ± 11.7	509	rejected
AA-50-1	Wire A + Ti wire	50 pct Ar-50 pct CO_2	268	257 ± 5.6	452	acceptable
AA-50-2	Wire A + Ti wire	50 pct Ar-50 pct CO_2	268	257 ± 5.6	480	acceptable
AA-50-3	Wire A + Ti wire	50 pct Ar-50 pct CO_2	268	257 ± 5.6	509	acceptable
B-30-1	Wire B	70 pct Ar-30 pct CO_2	267	259 ± 6.3	452	acceptable
B-30-2	Wire B	70 pct Ar-30 pct CO_2	267	259 ± 6.3	480	acceptable
B-30-3	Wire B	70 pct Ar-30 pct CO_2	267	259 ± 6.3	509	acceptable

(a) Macro photo for cracked specimen (A-30)

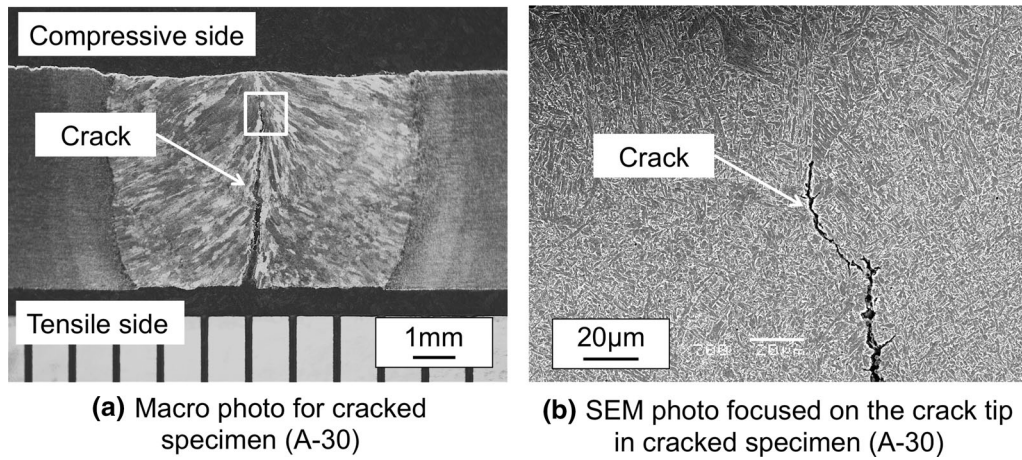**(b) SEM photo focused on the crack tip in cracked specimen (A-30)**

Fig. 3—Macro photo and SEM micrograph of specimen A-30 after SSC testing, (*a*) macro photo for cracked specimen (A-30), (*b*) SEM photo focused on the crack tip in cracked specimen (A-30).

Table III. Comparison of Specimen Hardness Before and After SSC Testing

Specimen ID	Hardness, 2 mm from Pipe Bottom Surface, HV1		Hardness, After SSC Test, 0.2 mm from Tensile Surface, HV0.5		Difference Before and After SSC			
	Maximum	Mean, $\pm \sigma$	Maximum	Mean, $\pm \sigma$	ΔMax	Avg. of Max $\pm \sigma$	ΔMean	Avg. of Mean $\pm \sigma$
A-30	258	251 ± 11.7	291	283 ± 8.5	33	33	32	32
AA-30-1	295	273 ± 11.7	330	295 ± 13.7	35	20.7 ± 12.7	22	22.7 ± 5.7
AA-30-2	295	273 ± 11.7	300	289 ± 6.6	5	20.7 ± 12.7	16	22.7 ± 5.7
AA-30-3	295	273 ± 11.7	317	303 ± 15.4	22	20.7 ± 12.7	30	22.7 ± 5.7
AA-50-1	268	257 ± 5.6	287	270 ± 8.2	19	16.0 ± 2.2	15	13.3 ± 1.2
AA-50-2	268	257 ± 5.6	282	257 ± 5.3	14	16.0 ± 2.2	13	13.3 ± 1.2
AA-50-3	268	257 ± 5.6	283	269 ± 7.5	15	16.0 ± 2.2	12	13.3 ± 1.2
B-30-1	267	259 ± 6.3	281	262 ± 11.8	14	10.3 ± 2.9	3	4.7 ± 2.4
B-30-2	267	259 ± 6.3	274	262 ± 7.4	7	10.3 ± 2.9	3	4.7 ± 2.4
B-30-3	267	259 ± 6.3	277	267 ± 7.1	10	10.3 ± 2.9	8	4.7 ± 2.4

orientation, with some white areas which suffered poor EBSD indexing shown in the left-hand figure (due to the previous presence of silver), and red dots which indicate silver. It should be noted that the silver particles are predominantly located at the locations of black lines, which correspond to high angle grain boundaries with more than 15 degree misorientations in the right-hand figure. It seems that the red dot, silver particle locations coincide with grain boundaries of acicular ferrite, while fewer silver particles were detected within the interior of grains. According to Koyama *et al.*,[21] high angle grain boundaries can trap hydrogen more than low angle grain boundaries, and the segregation and accumulation of hydrogen at grain boundaries increase with hydrogen flux. The present results are somewhat in support of this finding as well.

IV. DISCUSSION

From the SSC test results, SSC initiated in A-30 and all AA-30 series welds, although it did not initiate in A-50 series and B-30 series. AA-30 series had extremely high hardness exceeding 290 HV in terms of maximum hardness value although this weld metal contained a much higher IGF volume fraction. Based on the NACE and EFC standards discussed previously, the critical value which cannot be exceed is 250 HV. This is based on the principle that one must avoid local hard microconstituents with high hardness that will be prone to concentrating hydrogen and initiating a crack. In contrast, the average values of all the specimens tested here were fairly uniform and well above 250 HV, and thus one might expect that none of the weld metals should survive the SSC test. Yet, the specimens from the A-30, AA-50 series, and B-30 series had almost the same hardness values before SSC test, but only the A-30 specimen failed the SSC test, and so further consideration of the source of failure is required.

First of all, the volume fraction of IGF in specimen A-30 was low compared with others. As demonstrated in Figure 4, it can be noted that grain boundaries corresponding to IGF can trap diffusible hydrogen. Thus, if the IGF volume fraction is high, the capacity to trap diffusible hydrogen would be high. Wang *et al.* investigated the effect of acicular ferrite in submerged
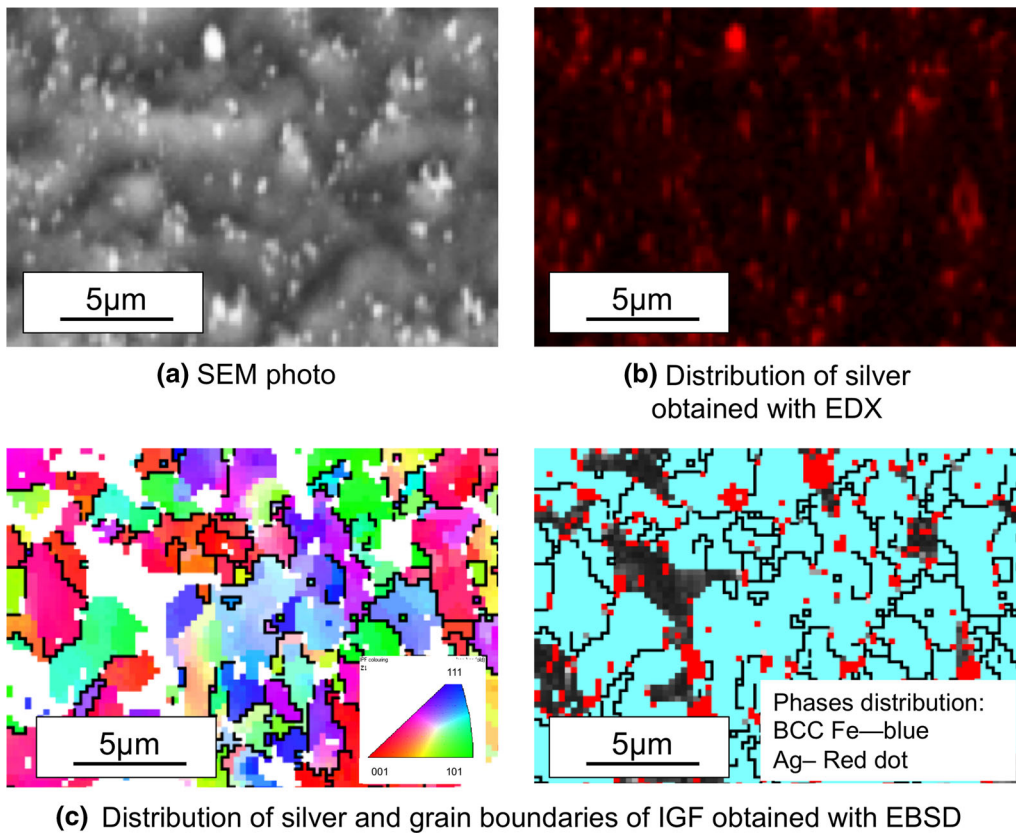
(a) SEM photo

(b) Distribution of silver obtained with EDX

(c) Distribution of silver and grain boundaries of IGF obtained with EBSD

Phases distribution:
BCC Fe—blue
Ag– Red dot

Fig. 4—Distribution of hydrogen trapping sites revealed by hydrogen microprint technique, (*a*) SEM photo, (*b*) distribution of silver obtained by EDX, (*c*) distribution of silver and grain boundaries of IGF obtained by EBSD.

arc weld metals on hydrogen trapping, and concluded that diffusible hydrogen can be trapped at grain boundaries in acicular ferrite.[15] Our results are consistent with theirs, although the welding processes are different. Furthermore, Zhao *et al.* have stated that nano-sized carbides within acicular ferrite act as hydrogen trapping sites.[22,23] Figure 5 is a photograph taken of an IGF grain boundary in A-30 by Transmission Electron Microscopy (TEM). This specimen was extracted from the root area, processed by *in-situ* lift-out using ion milling, and the IGF microstructure analyzed by bright field TEM. From the results it can be noted that some nano-sized precipitates are found in the IGF microstructure. Those precipitates are similar in terms of location, size, and distribution compared with the results by Zhao *et al.*[22,23] Therefore, it is expected that those precipitates are carbides and their role in trapping diffusible hydrogen is similar. Hence, it is suggested that rich nano-scale carbides in the IGF regions will reduce SSC susceptibility.

On the other hand, A-30 contains a much higher fraction of GBF compared with AA-50 and B-30, and SSC propagated mainly along prior austenitic grain boundaries as illustrated in Figure 3. Thus, the effects of GBF on SSC susceptibility should be also considered. The following two possible reasons are proposed to explain why the microstructure involving more GBF is vulnerable to SSC. First, the grain size of GBF is larger than IGF, so that local fracture toughness could be
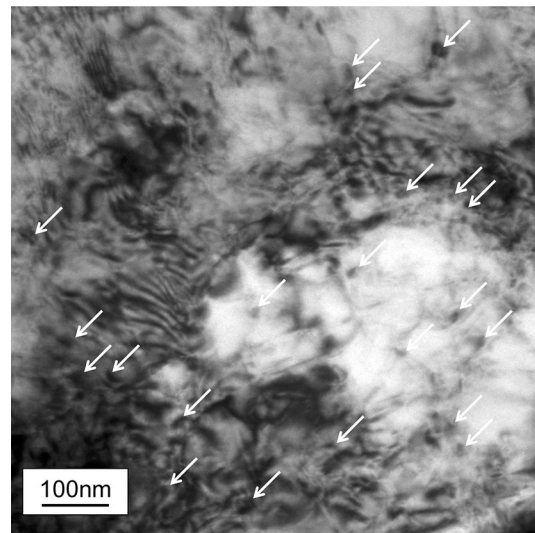

Fig. 5—Carbides observed by TEM in specimen A-30.

inferior. Secondly, if local yielding occurs, dislocations which can carry diffusible hydrogen might be concentrated in the GBF especially around the crack during SSC testing because GBF is typically low strength comparing with IGF. If so, GBF could become brittle preferentially by acquiring a high diffusible hydrogen concentration during SSC testing. The difference in
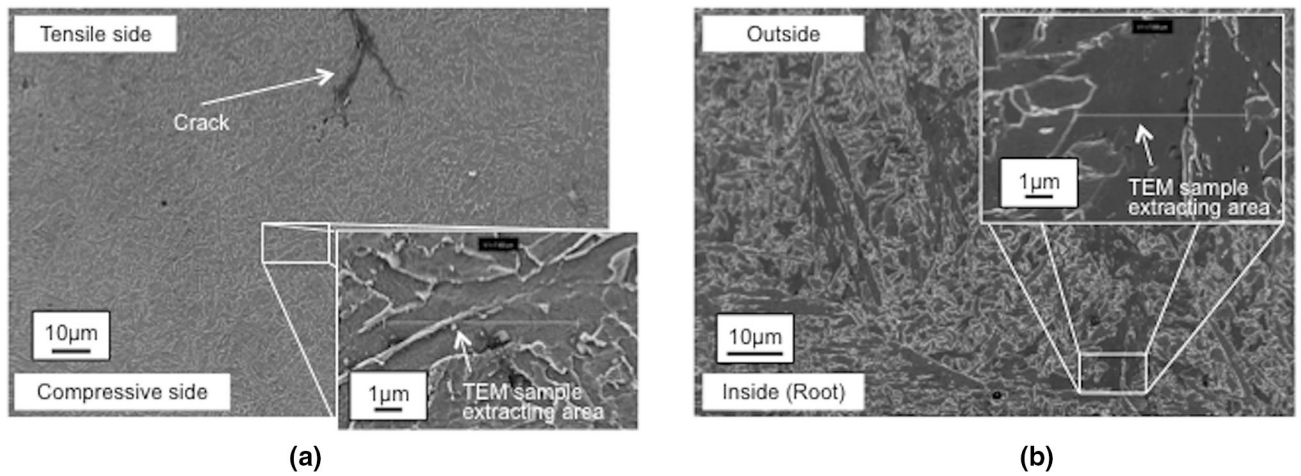
Fig. 6—TEM sample locations prepared by ion beam milling, (a) TEM sample extracted location near crack tip in A-30, (b) TEM sample extracted location near tensile side in the virgin specimen.

(a) A GBF near crack tip
in the cracked specimen

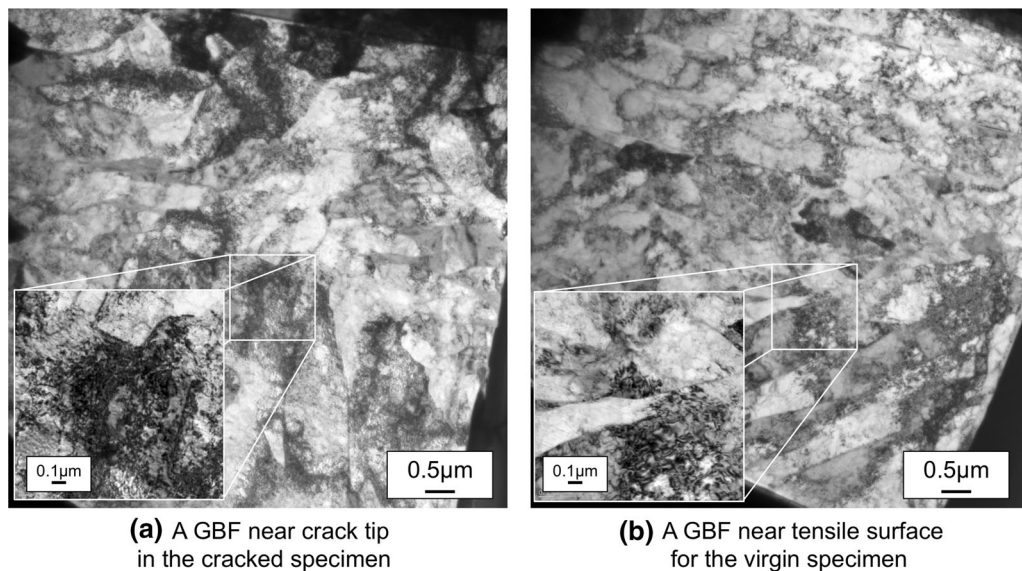**(b)** A GBF near tensile surface
for the virgin specimen

Fig. 7—Comparison of dislocations at a location of grain boundary ferrite, (a) a grain boundary ferrite at near crack tip in the cracked specimen, (b) a grain boundary ferrite at near tensile surface for the virgin specimen.

dislocation density in the GBF of the weld both before SSC testing (at the root area, 2 mm from inner surface), and near a crack tip after SSC, were examined to evaluate this second possibility. The precise positions for the sample extractions are illustrated in Figure 6, as observed by SEM.

The bright field micrographs for each location are shown in Figure 7. It seems that the dislocation density in GBF at the SSC crack tip is either marginally higher or similar compared to the as-welded material. Thus, the mechanism describing the enhanced diffusion of hydrogen *via* an increased concentration of dislocations within the GBF could not be confirmed. Hence, the results suggest that the main reason that GBF is significantly weaker than IGF stems from the inherent low local fracture toughness in the GBF derived from a coarser

grain size. Lopez et al.[24] reported that, for API 5L X80 pipeline steels, SSC propagated among prior austenitic grain boundaries. They stated that certain impurities, such as phosphorous are typically brittle, segregate at grain boundaries, and facilitate crack propagation along the grain boundaries. This supports the claim that GBF exhibits a low fracture toughness compared to IGF. As mentioned above, it was observed that specimen A-30, which incorporated more GBF, exhibited a lower SSC resistance compared with specimens AA-50 and B-30. This suggests that decreasing the volume fraction in GBF is desirable in order to increase SSC resistance.

Finally, the comparison between B-30 series and AA-50 series is worth examining. As shown in Table I, both were deemed acceptable by the SSC tests. B-30 series welds contained less carbon than the AA-50 series.

Moreover, Pcm value for B-30 and AA-50, which is index to evaluate hydrogen crack susceptibility are 0.20 and 0.23, respectively, where the Pcm value is calculated using the following equation[25]

$$Pcm = C + Si/30 + Mn/20 + Cu/20 + Ni/60 + Cr/20 + Mo/15 + V/10 + 5B \text{ (wt pct)}$$

Additionally, as shown in Table II, the change in hardness after SSC testing was less pronounced for the B-30 series than the AA-50 series. It has been reported that lower carbon contents result in higher hardenability.[26,27] Thus, B-30 might have a stronger SSC resistance than AA-50 due to a lower carbon and Pcm value. However, a more aggressive or prolonged test may be needed to verify this.

V. CONCLUSIONS

In this paper, SSC susceptibility for weld metals with various intragranular ferrite volume fractions, and the role of microstructure in terms of SSC susceptibility, were investigated.

1. Welds with the highest intragranular ferrite to grain boundary ferrite ratio passed SSC tests although the hardness values exceeded 250 HV, the threshold guideline to prevent SSC initiation.
2. It was confirmed that grain boundaries of intragranular ferrite play a role as the key hydrogen trapping sites due to the fine grain structure and finely dispersed nano-scale carbonitride precipitates.
3. Microstructure involving much grain boundary ferrite is potentially weaker than microstructure dominating intragranular ferrite due to local fracture toughness between microstructures deriving from grain size. Grain boundary ferrite has a lower local fracture toughness, due in part to its grain size, than intragranular ferrite. Therefore materials that are relatively rich in intragranular ferrite are less susceptible to SSC testing than those containing more grain boundary ferrite.

REFERENCES

1. NACE MR0175/ISO 15156 Petroleum and Natural Gas Industries—Materials for Use in H_2S—Containing Environments in Oil and Gas Production.
2. European Federation of Corrosion Publication Number 16—Guidelines on Materials Requirements for Carbon and Low Alloy Steels for H_2S-Containing Environments in Oil and Gas Production.
3. B. Beidokhiti, P. He, A.H. Kokabi, and A. Dolati: *Mater. Sci. Technol.*, 2017, vol. 33 (4), pp. 408–14.
4. G.M. Omweg, G.S. Frankel, W.A. Bruce, J.E. Ramirez, and G. Koch: *Corrosion*, 2003, vol. 59 (7), pp. 640–53.
5. F. Huang, S. Liu, J. Liu, K.G. Zhang, and T.H. Xi: *Mater. Sci. Eng. A*, 2014, vol. 591, pp. 159–66.
6. L. Gan, F. Huang, X. Zhao, J. Liu, and F.F. Cheng: *Int. J. Hydrogen Energy*, 2017, https://doi.org/10.1016/j.ijhydene.2017.11.155.
7. H. Asahi and M. Ueno: *ISIJ Int.*, 1994, vol. 34 (3), pp. 290–94.
8. H. Asahi, M. Ueno, and T. Yonezawa: *Corrosion*, 1994, vol. 50 (7), pp. 537–45.
9. T. Sourmail and G. Abington: *International Corrosion Conference*, NACE, 2007, paper 07104.
10. T. Omura, K. Kobayashi, and M. Ueda: *International Corrosion Conference*, NACE, 2009, paper 09102.
11. K. Kobayashi, T. Omura, N. Takahashi, I. Minato, and A. Yamamoto: *Proceedings of the 8th International Pipeline Conference*, IPC2010, 2010, paper 31106.
12. M. Al-Mansour, A.M. Alfantazi, and M. El-boujdaini: *Mater. Des.*, 2009, vol. 30, pp. 4088–94.
13. B. Beidokhti, A. Dolati, and A.H. Koukabi: *Mater. Sci. Eng.*, 2009, vol. 507A (1), pp. 167–73.
14. T. Kasuya, J. Kobayashi, S. Ohkita, and M. Fuji: *Sci. Technol. Weld. Join.*, 1998, vol. 3 (1), pp. 25–32.
15. S.H. Wang, W.C. Luu, K.F. Ho, and J.K. Wu: *Mater. Chem. Phys.*, 2003, vol. 77 (2), pp. 447–54.
16. ASTM G39: *Standard Practice for Preparation and Use of Bent-Beam Stress-Corrosion test Specimens*, ASTM, West Conshohocken, 2016.
17. J. Ovejero-García: *J. Mater. Sci.*, 1985, vol. 20 (7), pp. 2623–29.
18. K. Ichitani, M. Kanno, and S. Kuramoto: *ISIJ Int.*, 2003, vol. 43 (4), pp. 496–504.
19. K. Ichitani, S. Kuramoto, and M. Kanno: *Corros. Sci.*, 2003, vol. 45 (6), pp. 1227–34.
20. K. Ichitani and M. Kanno: *Sci. Technol. Adv. Mater.*, 2003, vol. 4 (6), pp. 545–51.
21. M. Koyama, D. Yamasaki, T. Nagashima, C.C. Tasan, and K. Tsuzaki: *Scr. Mater.*, 2017, vol. 129, pp. 48–51.
22. M.C. Zhao, M. Liu, A. Atrens, Y.Y. Shan, and K. Yang: *Mater. Sci. Eng.*, 2008, vol. 478A (1–2), pp. 43–47.
23. M.C. Zhao and K. Yang: *Scr. Mater.*, 2005, vol. 52, pp. 881–86.
24. H.F. Lopez, R. Raghunath, J.L. Albarran, and L. Martinez: *Metall. Mater. Trans. A*, 1996, vol. 27, pp. 3601–11.
25. The Japan Welding Engineering Society. http://www-it.jwes.or.jp/weld_simulator/en/cal4.jsp. Accessed 5 Aug 2018.
26. H. Asahi: *Zairyo-to-Kankyo*, 2000, vol. 49 (4), pp. 201–08 (Japanese).
27. M. Hamada: *J. Jpn. Weld. Soc.*, 2011, vol. 49 (4), pp. 201–08 (Japanese).